THE INFLUENCE OF DIFFERENT WING MOTIONS ON THE LIFT IN BIO-INSPIRED AERIAL VEHICLES

Bianca Taís Visoná Carnielo[1] & Douglas D. Bueno[1]

[1]São Paulo State University (UNESP) - School of Engineering, Ilha Solteira, SP, Brazil

Abstract

With the recent applications of micro aerial vehicles for civil and military use, the interest in non conventional aerodynamic designs is growing, in this context, the bio-inspired aerial vehicles show some advantages when compared with the fixed and rotary-wings aircraft, such as noise reduction, efficiency and reduced size. Identifying the aerodynamic principles that allow species of birds, insects and bats to fly can bring tools for aircraft development, since these species make use of aerodynamic principles different from those used in engineering. Once one of the challenges of building bio-inspired UAVs (unmanned aerial vehicles) is modeling the aerodynamics of flapping wings, the present work uses the UVLM (Unsteady Vortex Lattice Method) to obtain the aerodynamic forces and pressure values for two different wings configuration inspired by the Great black-backed gull (*Larus marinus*) and by the Blue-and-yellow macaw (*Ara Ararauna*). The influence of the wing movements of flapping, pitching, heaving and spanning and folding on the aerodynamic performance of the wing is analyzed through the lift and thrust/drag coefficients.

Keywords: bio-inspired, UVLM, flapping wings, UAV, aerodynamic

1. Introduction

The flapping of wings provides the ability of flying for thousands of species of insects, birds and bats, many species even cross the globe annually in the process of migration. Identifying the aerodynamic principles that allow these species to fly can bring tools for aircraft development, since the species make use of aerodynamic principles different from those used in engineering [1]. With the recent applications of micro aerial vehicles for civil and military use, the aerodynamic performance of fixed-wing aircraft does not achieves the best results at low Reynolds number conditions, the practicality of rotary-wing aircraft is also limited due to the generation noise, susceptibility to the effects of proximity to walls and inefficiency at low Reynolds numbers [2]. [3] show that insect-like flapping devices are twice as efficient as rotating wings when hovering at a Reynolds number below 100.

One of the challenges of building bio-inspired UAVs (unmanned aerial vehicles) is modeling the aerodynamics of flapping wings. To this end, [4] compare the ability of a low-fidelity model based on the inviscid Doublet Lattice panel method and a high-fidelity model based on the Navier-Stokes equations to numerically simulate the flapping of MAVs (micro aerial vehicles), the results show that, in many cases, low-fidelity simulations are able to satisfactorily predict the forces and indicate regions of possible flow separation, even though the high-fidelity method is indicated to obtain greater flow details.

Another method used is the UVLM (unsteady vortex lattice method), a medium fidelity panel method that consists of assigning vortex rings and a collocation point to each panel and includes the modeling of wing-wake interaction. [5] present a historical review of the methodology, how this method can be used as an alternative to methods such as DLM (doublet lattice method) and strip theory for problems that include the dynamics of flexible structures, the authors also emphasize the advantages of this method in modeling non-stationary aerodynamics in vehicles with aeroelasticity coupled to flight dynamics and surfaces under the action of complex kinematics or large deformations. [6]

developed an extension to the UVLM in order to study the aerodynamics of insect wings, the authors use models to improve the modeling of the wing-wake interaction and the effects of the leading edge vortex, the results show that the developed methodology can efficiently simulate the non-stationary aerodynamics of insects with advantages when compared to previous UVLMs.
This method is widely used in the literature, mainly in the context of flapping aerodynamics [7, 8, 9, 10]. [11] present a method to analyze the flapping wings of bio-inspired water vehicles that includes coupling flexible multibody dynamics to the UVLM for hydrodynamic modeling. [12] use the UVLM to model non-stationary aerodynamics in the study of trajectory optimization of FWMAVs (flapping wing micro air vehicles). [13] present a study to optimize the shape of flapping wings, the analysis is carried out by combining the UVLM with a gradient-based optimizer. The UVLM is also used in other contexts such as wind turbines [14], aeroelastic analysis and flutter prediction in structures with geometric non-linearities [15] and in simulating the flow around bio-inspired nano rotors [16].
In this context, the present work uses the UVLM to obtain the aerodynamic forces and pressure values for two different wing configuration inspired by the Great black-backed gull (*Larus marinus*) and by the Blue-and-yellow macaw (*Ara Ararauna*). The influence of the wing movements of flapping, pitching, heaving and spanning and folding on the aerodynamic performance of the wing is analyzed through the lift and thrust/drag coefficients.

2. The Unsteady Vortex Lattice Method

The UVLM consists of discretizing the lift surfaces using panels, each panel has an associated vortex ring, quadrilateral elements composed of discrete vortex segments in a closed loop. The leading segment of the ring is positioned on the first quarter chord of the panel to satisfy the Kutta's condition, which says that the flow must gently detach at the trailing edge to form the wake, this condition is imposed to remove the indeterminacy regarding the circulation around the body, leading to a unique solution. The collocation points are located in the center of the $3/4$ line of the panel, a normal vector located at this point is then defined.
In a given time step, the impermeability condition is imposed at each collocation point, this condition is translated mathematically by canceling the vertical component of the local velocity at the collocation point of each panel, like is shown in Equation 1

$$A_b^{n+1}\Gamma_b^{n+1} + A_w^{n+1}\Gamma_w^{n+1} + w^{n+1} = 0 \tag{1}$$

where Γ_b^{n+1} and Γ_w^{n+1} are the circulation induced by the vortex rings of the bound and wake, respectively, A_b^{n+1} and A_w^{n+1} are the matrices of influence of the bound vortex and wake vortex, respectively and w^{n+1} are the velocities not induced by vortices (free flow and flapping wings velocities).
The elements of the matrices A_b^{n+1} and A_w^{n+1} are computed by using the Biot-Savart law. First of all, it is computed the velocities induced by each side of an j-th vortex ring in the i-th panel, that is given by

$$a_{b_{ij}}^{(p,q)} = \frac{1}{4\pi}\frac{(\vec{r}_p)_{ij}\times(\vec{r}_q)_{ij}}{|(\vec{r}_p)_{ij}\times(\vec{r}_q)_{ij}|^2}\left[(\vec{r}_p - \vec{r}_q)_{ij}\bullet\left(\frac{(\vec{r}_p)_{ij}}{|(r_p)_{ij}|} - \frac{(\vec{r}_q)_{ij}}{|(r_q)_{ij}|}\right)\right] \tag{2}$$

where (p,q) is equal to $(1,2)$, $(2,3)$, $(3,4)$ e $(4,1)$ and represents the sides of the vortex ring. The total influence of a vortex ring is the sum of the influences of each side, such that

$$a_{b_{ij}} = \sum_{p=1}^{4} a_{b_{ij}}^{(p,q)} \tag{3}$$

The same procedure is done for all bound vortex and wake vortex. The Figure 1 shows the evaluation of the influence of the j-th panel vortex ring on the collocation point of the i-th panel.
The strength of the vortices shed by the surface and forming the wake are equal to the intensities of the trailing edge vortices in the previous time step, that is, $\Gamma_w^{n+1} = \Gamma_{te}^{n}$. Therefore, all parameters of Equation 1 are known except Γ_b^{n+1}, that can be computed once it is a linear equation system.
Once the vortex strength of all panels are known, it is possible to determine the velocity field and the aerodynamic forces, the forces are computed through the Joukowski method. According to [17], in the Joukowski method, the total force is divided into quasi-steady and unsteady. Since $\vec{l}_{pi}$ is one side

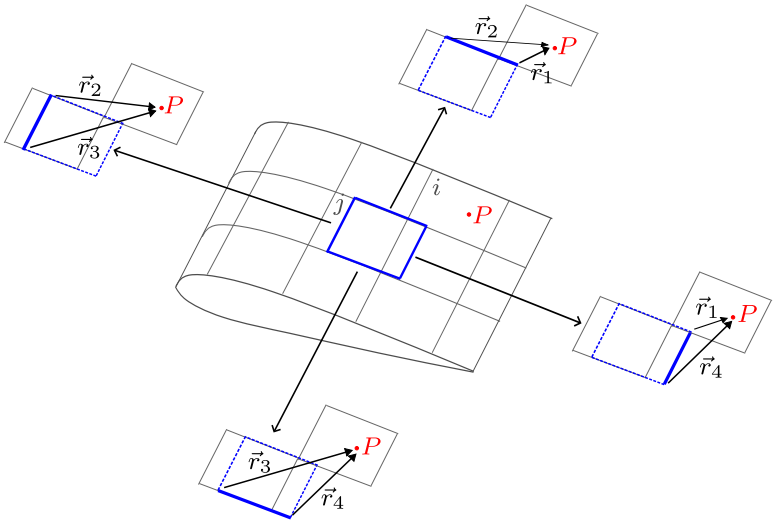

Figure 1 – Evaluation of the influence of a vortex ring on a collocation point.

of the i-th vortex ring (with $p = 1,\ 2,\ 3$ and 4), it has a velocity $\vec{V}_{pi}$ at its center and a circulation Γ_{pi}, this circulation is the same for all sides of a ring, therefore $\Gamma_{pi} \equiv \Gamma_i$. Furthermore, the vector $\vec{l}_{pi}$ can be obtained by $\vec{l}_{pi} = (\vec{r}_p - \vec{r}_q)_{ij}$ whatever panels i and j are. Then, the steady contribution of this vortex segment to the force is calculated by

$$\vec{F}_{pi}^{st} = \rho\Gamma_{pi}(\vec{V}_{pi} \times \vec{l}_{pi}) \tag{4}$$

So that the contribution of a ring is given by $\vec{F}_i^{st} = \sum_{p=1}^{4} \vec{F}_{pi}^{st}$. Note that the impermeability condition is imposed only at the control points, so that $\vec{V} \times \vec{l}$ does not necessarily act in the direction normal to the panel. The unsteady contribution comes from the unsteady Bernoulli equation, it acts in the normal direction of each panel. With ρ being the density of the fluid, $\frac{\partial \Gamma_i}{\partial t}$ the variation of circulation in time, S_i the area and $\vec{n}_i$ the normal vector of the i-th panel, the unsteady portion of the force is given by

$$\vec{F}_i^{unst} = \rho \frac{\partial \Gamma_i}{\partial t} S_i \vec{n}_i \tag{5}$$

where the normal vector is obtained by $\frac{\vec{l}_{pi} \times \vec{l}_{(p+1)i}}{|\vec{l}_{pi} \times \vec{l}_{(p+1)}|}$. The variation of circulation in time is the ratio between the difference in circulation in a time step and the previous time step $\Gamma_i^{n+1} - \Gamma_i^n$ and the time step Δt. Thus, the total contribution of the i-th panel is $\vec{F}_i^{tot} = \vec{F}_i^{st} + \vec{F}_i^{unst}$.
The pressure can be determined by

$$p_i = \frac{\vec{F}_i^{tot} \cdot \vec{n}_i}{S_i} \tag{6}$$

3. Results and Discussion

This study uses two different wing geometry that are inspired by the Great black-backed gull (*Larus marinus*) [18, 19] and by the Blue-and-yellow macaw (*Ara Ararauna*) [20], the geometries are shown respectively in the Figure 2 and Figure 3. Moreover, the free flow velocity used for the first case is 12m/s and for the second case is 6m/s.
According to [21] wing flapping consists of four basic motions: an up and down motion (flapping) of the entire wing, a rotation (pitching) of the wing with a negative pitch-down pronation during the downstroke and a positive pitch-up supination during the upstroke, an angular motion of the entire wing forward and backward (heaving), and an alternatively extending and contracting of the wing (spanning and folding).
These four movements and the combination of them are reproduced for both geometries, the flap movement has an amplitude of $45°$, the pitch movement has a pronation of $5°$ and supination of $15°$, the heave movement has an amplitude of $15°$ and the fold movement is done by the cross section in the middle of the wing semi-span with an angle of $45°$. The movements frequency is 3Hz.

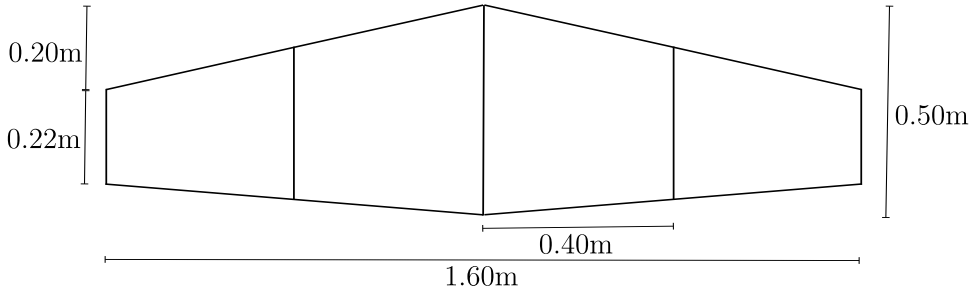

Figure 2 – Wing geometry inspired by the Great black-backed gull.

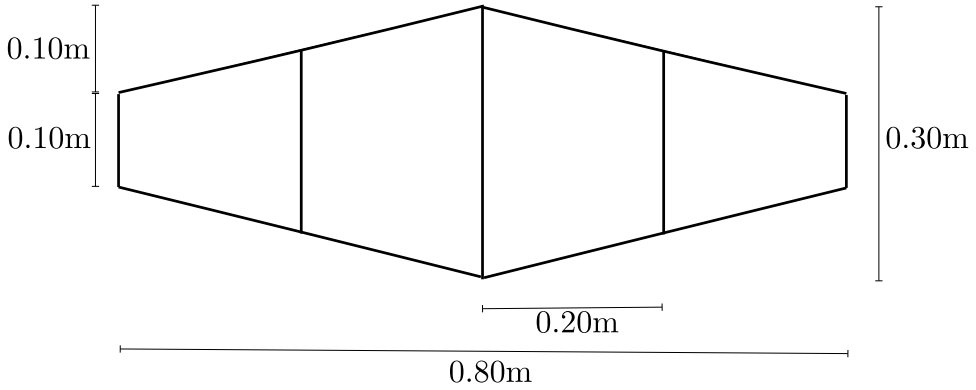

Figure 3 – Wing geometry inspired by the Blue-and-yellow macaw.

Each wing has 384 panels. The aerodynamic profile used is the NACA0012. For both wings is obtained the lift and drag coefficients and the pressure in the panel located at the tip of the leading edge. The time simulated is of three cycles of motion and the flapping movement is included in all simulations, the Figure 4 shows the flapping motion over time.

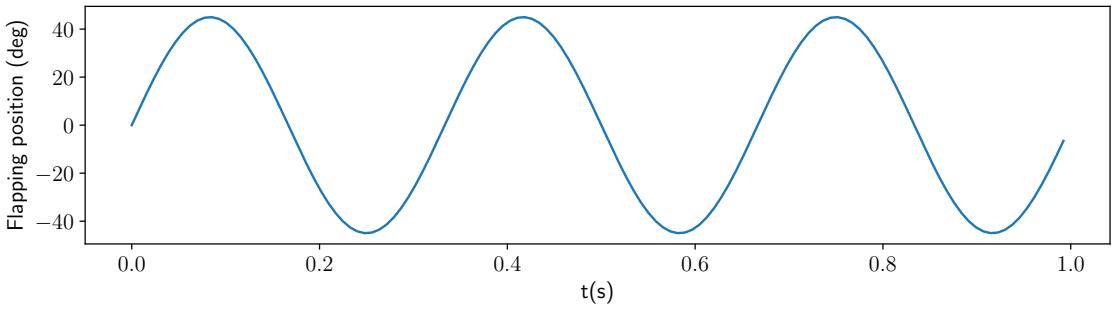

Figure 4 – Flapping motion over time.

The Figure 5 shows the lift coefficient for the geometry inspired by the Blue-and-yellow macaw. During one cycle of the wing flap, there is a gain and a loss of lift, it is wanted the net lift to be positive, the flap movement alone (blue solid line) has a higher loss of lift, the flapping motion with pitch and with all movements combined presents a lower loss of lift. The same behavior can be seen for the geometry inspired by the Great black-backed gull in Figure 6.

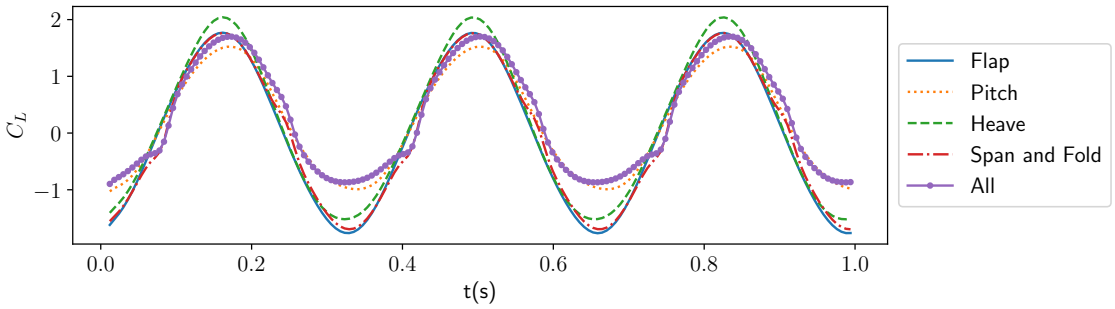

Figure 5 – Lift coefficient over time for different wings motion inspired by the Blue-and-yellow macaw.

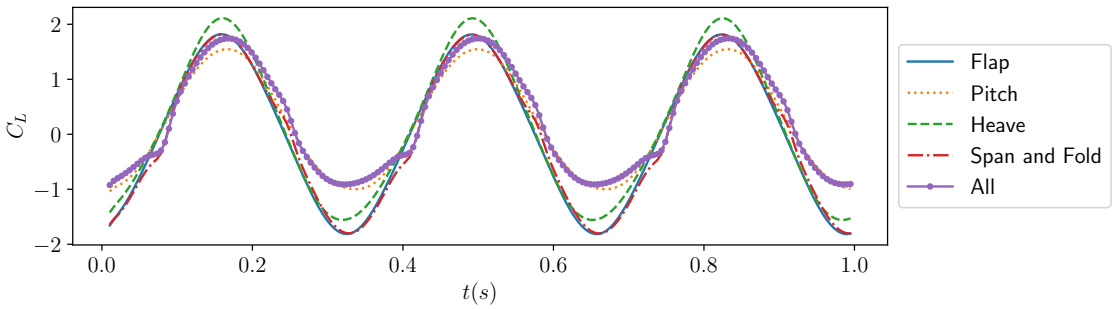

Figure 6 – Lift coefficient over time for different wings motion inspired by the Great black-backed gull.

The Table 1 shows the mean value of the lift coefficient for all motions and both geometries.

Movement	Gull	Macaw
Flap	0.0172	0.0160
Pitch	0.2279	0.2196
Heave	0.1670	0.1530
Span and Fold	0.0144	0.0301
All	0.3004	0.2945

Table 1 – Mean lift coefficient for each motion.

The pitch motion is, therefore, responsible for the gain of lift. Moreover, lift coefficients are higher for the Great black-backed gull than the Blue-and-yellow macaw, except for span and fold motions, so this kind of motion may be not efficient for all wing geometries. The drag coefficients are shown in Figures 7 and 8.

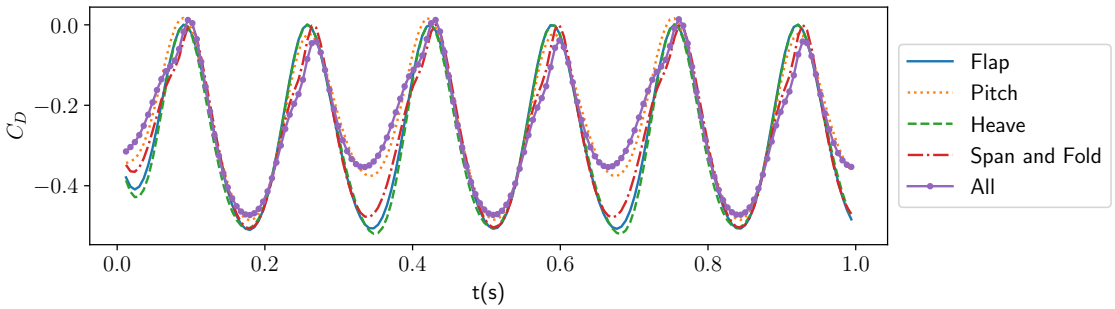

Figure 7 – Drag coefficient over time for different wings motion inspired by the Blue-and-yellow macaw.

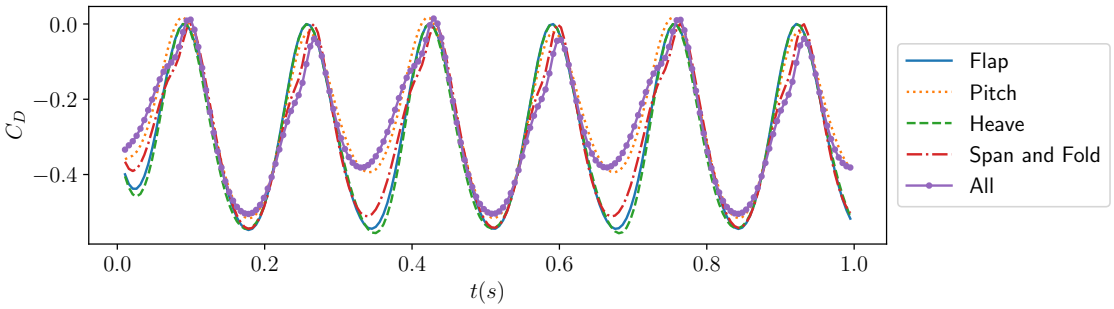

Figure 8 – Drag coefficient over time for different wings motion inspired by the Great black-backed gull.

Negative values of the drag coefficients indicate thrust generation, in this case, better values of drag coefficient are the lowest. The Figures 7 and 8 show that the flapping alone and with heave motion present the lowest values of drag coefficient. But to confirm the influence of these motions it is necessary to analyze the mean values that are shown in Table 2. It can be seen that the mean drag coefficient is not significantly lower for the Great black-backed gull when compared with the Blue-and-yellow Macaw. Also, the heave and flap motion are the most responsible for the thrust generation.

Movement	Gull	Macaw
Flap	-0.2908	-0.2706
Pitch	-0.2500	-0.2359
Heave	-0.2982	-0.2777
Span and Fold	-0.2914	-0.2715
All	-0.2634	-0.2462

Table 2 – Mean drag coefficient for each motion.

When comparing the flap motion (Figure 4) with the lift coefficients (Figures 5 and 6), note that the positive lift values happen during the downstroke and the negative lift values during the upstroke. And when comparing the flap motion with the drag coefficient (Figures 7 and 8), note that the highest drag coefficient values happen when the wing is positioned at the limits of $45°$ and $-45°$ of amplitude. The Figures 9 and 10 show the pressure in the panel located at the tip of the leading edge, the results show that for the span and fold motion the pressure values presents a lower negative peak, this means that the angulation of the tip of the wing develops the role of decreasing the loss of lift during the flapping cycle, mainly for the blue-and-yellow macaw.

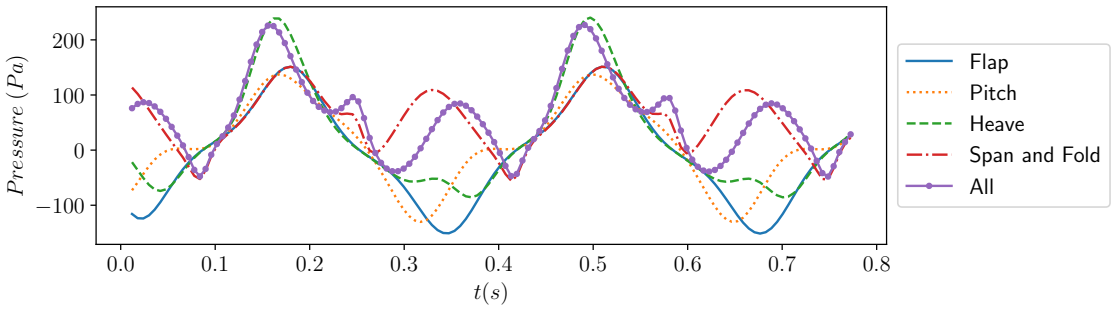

Figure 9 – Pressure in the panel located at the tip of the leading edge over time for different wings motion inspired by the Blue-and-yellow macaw.

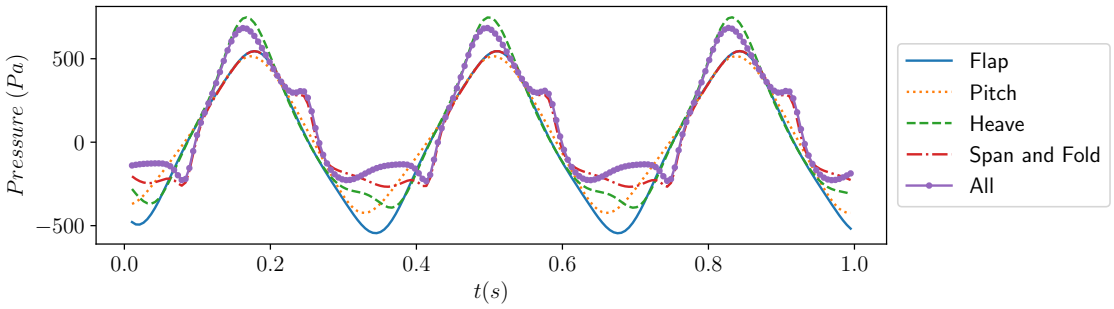

Figure 10 – Pressure in the panel located at the tip of the leading edge over time for different wings motion inspired by the Great black-backed gull.

Aiming to define the most convenient type of motion, in terms of the amplitude and frequency of flapping, for a particular dimension and geometry of wing, the blue-and-yellow macaw geometry is used, once the results for lift and drag for this case show a better relation between forces and dimension. Four amplitudes are considering for a frequency of 3Hz, the lift results are in Figure 11 and the drag results are in Figure 12.

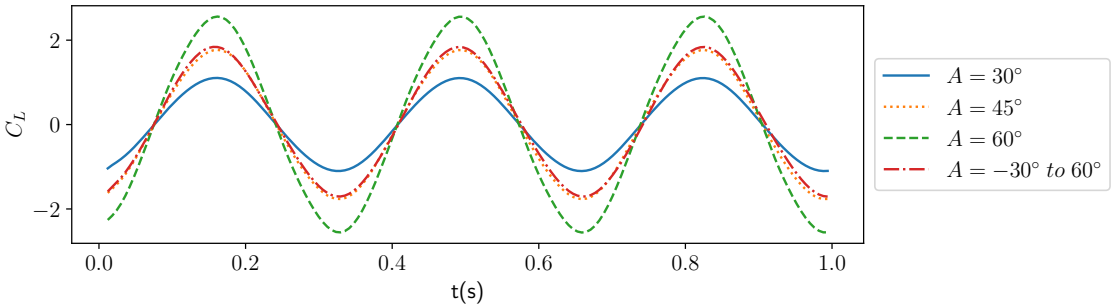

Figure 11 – Lift coefficient over time for different flapping amplitudes.

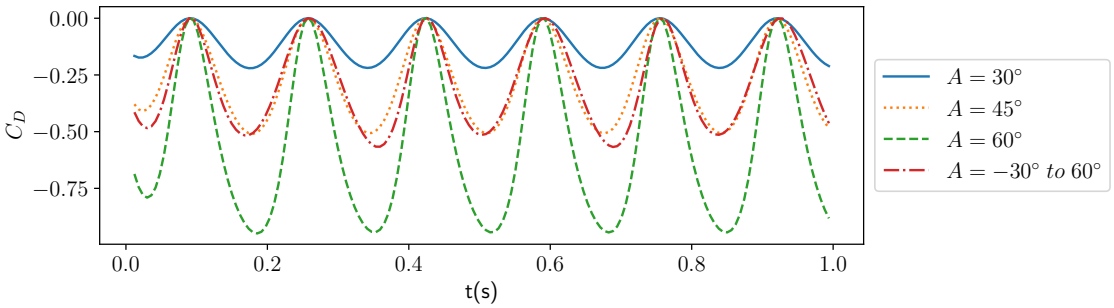

Figure 12 – Drag coefficient over time for different flapping amplitudes.

To increase the amplitudes do not mean a better results in terms of lift, the positive peak is higher but so is the negative peak. The use of an asymmetric flapping does not show a significantly change. Considering the drag coefficient, the increase in amplitudes show an important role for improving the results. The frequency is other parameter analyzed, the results for lift and drag are shown in Figures 13 and 14, respectively. In this case, higher frequency values also mean better results for drag. The isolated flapping motion is not sufficient to improve the lift results, it is necessary to include the other motions.

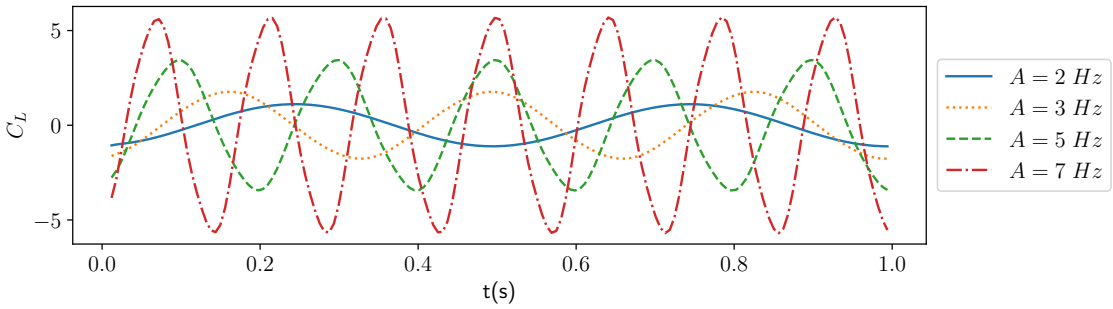

Figure 13 – Lift coefficient over time for different flapping frequencies.

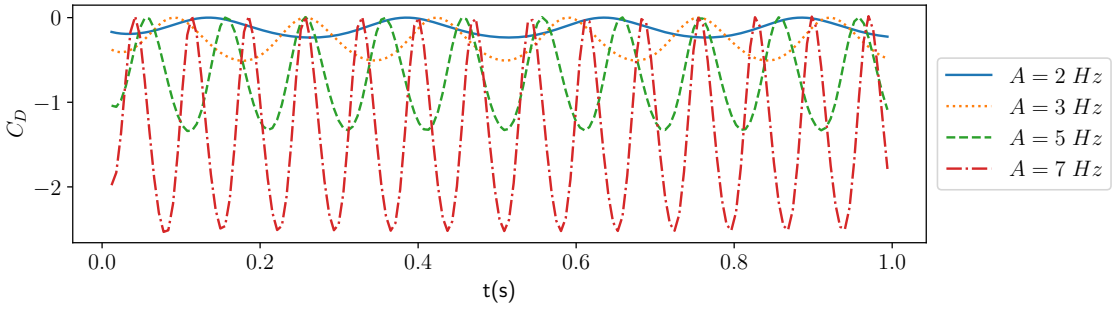

Figure 14 – Drag coefficient over time for different flapping frequencies.

4. Conclusions

This type of UAV exhibits advantage in comparison with the classical fixed-wing aerial vehicle. However, there several challenges to be overcome in order to establish a robust procedure for designing flapping-wing-based UAV. There are several parameters that can influence the aerodynamic of these UAVs such as motions, amplitudes, frequencies and geometries. Aiming to clarify the influences of some of these parameters, this work study the motions of flapping, pitching, heaving and spanning and folding, and also the amplitude and frequency of flapping motion. The results show that each kind of motion has a role to play in the flapping flight, pitch, for example, is important for lift generation, but can do the drag coefficient worse. In the case of heave, the motion is helpful for thrust generation. The span and fold motion show to be dependent of the wing geometry, once for the blue-and-yellow macaw it improved the lift results but does not the same for the Great black-backed gull. So, it is important to have a clear goal, if it is thrust or lift, because the best motion for one can be the worts for other. The results of the flapping analyses show that this motion needs the others to achieve a positive net lift, even changing the frequency and amplitude. Although the drag results are better for higher amplitudes and frequencies.

5. Acknowledgments

The authors appreciate the support under Grant numbers: 2023/04325-3 and 2022/03128-7 from the São Paulo Research Foundation (FAPESP). The second author thanks to the National Council for Scientific and Technological Development (CNPq) grant number 314151/2021-4.

6. Contact Author

Mail to: bianca.carnielo@unesp.br
Tel: +55017991346311
Address: Rua Remanso, 200 - Ilha Solteira-SP, Brazil

7. Copyright Statement

References

[1] Diana D. Chin and David Lentink. Flapping wing aerodynamics: from insects to vertebrates. *Journal of Experimental Biology*, 219(7):920–932, April 2016.

[2] Y J Lee, K B Lua, T T Lim, and K S Yeo. A quasi-steady aerodynamic model for flapping flight with improved adaptability. *Bioinspiration &; Biomimetics*, 11(3):036005, April 2016.

[3] L Zheng, T Hedrick, and R Mittal. A comparative study of the hovering efficiency of flapping and revolving wings. *Bioinspiration & Biomimetics*, 8(3):036001, May 2013.

[4] P.-O. Persson, D.J. Willis, and J. Peraire. Numerical simulation of flapping wings using a panel method and a high-order navier–stokes solver. *International Journal for Numerical Methods in Engineering*, 89(10):1296–1316, February 2012.

[5] Joseba Murua, Rafael Palacios, and J. Michael R. Graham. Applications of the unsteady vortex-lattice method in aircraft aeroelasticity and flight dynamics. *Progress in Aerospace Sciences*, 55:46–72, November 2012.

[6] Anh Tuan Nguyen, Joong-Kwan Kim, Jong-Seob Han, and Jae-Hung Han. Extended unsteady vortex-lattice method for insect flapping wings. *Journal of Aircraft*, 53(6):1709–1718, November 2016.

[7] Joseph Reade and Mark Jankauski. Investigation of chordwise functionally graded flexural rigidity in flapping wings using a two-dimensional pitch–plunge model. *Bioinspiration &; Biomimetics*, 17(6):066007, October 2022.

[8] Anh Tuan Nguyen, Jae-Hung Han, and Thanh Trung Vu. The effects of wing mass asymmetry on low-speed flight characteristics of an insect model. *International Journal of Aeronautical and Space Sciences*, 20(4):940–952, May 2019.

[9] Anh Tuan Nguyen and Jae-Hung Han. Wing flexibility effects on the flight performance of an insect-like flapping-wing micro-air vehicle. *Aerospace Science and Technology*, 79:468–481, August 2018.

[10] Thomas Lambert, Norizham Abdul Razak, and Grigorios Dimitriadis. Vortex lattice simulations of attached and separated flows around flapping wings. *Aerospace*, 4(2):22, April 2017.

[11] Ming Luo, Zhigang Wu, and Chao Yang. Strongly coupled fluid–structure interaction analysis of aquatic flapping wings based on flexible multibody dynamics and the modified unsteady vortex lattice method. *Ocean Engineering*, 281:114921, August 2023.

[12] Sang-Gil Lee, Hyeon-Ho Yang, Reynolds Addo-Akoto, and Jae-Hung Han. Transition flight trajectory optimization for a flapping-wing micro air vehicle with unsteady vortex-lattice method. *Aerospace*, 9(11):660, October 2022.

[13] Mehdi Ghommem, Nathan Collier, Antti H. Niemi, and Victor M. Calo. On the shape optimization of flapping wings and their performance analysis. *Aerospace Science and Technology*, 32(1):274–292, January 2014.

[14] Wonsuk Han, Homin Kim, Eunkuk Son, and Soogab Lee. Assessment of yaw-control effects on wind turbine-wake interaction: A coupled unsteady vortex lattice method and curled wake model analysis. *Journal of Wind Engineering and Industrial Aerodynamics*, 242:105559, November 2023.

[15] Natsuki Tsushima, Hitoshi Arizono, and Masato Tamayama. Geometrically nonlinear flutter analysis with corotational shell finite element analysis and unsteady vortex-lattice method. *Journal of Sound and Vibration*, 520:116621, March 2022.

[16] Zhao Shanyong, Liu Zhen, Sun Yachuan, Dang Tianjiao, and Li Shiqi. Bio-inspired nano rotor investigation based on uvlm. *Biosurface and Biotribology*, 6(1):20–24, February 2020.

[17] Thomas Lambert. Modeling of aerodynamic forces in flapping flight with the unsteady vortex lattice method, 2015.

[18] C. J. Pennycuick. Speeds and wingbeat frequencies of migrating birds compared with calculated benchmarks. *The Journal of Experimental Biology*, 2001.

[19] Klaus Malling Olsen and Hans Larsson. *Gulls of Europe, Asia and North America*. A&C Black Publishers Ltd., 2010.

[20] S. Bhargavi, S. Venkatesan, Geetha Ramesh, and T.A. Kannan. Morphometrical analysis of the wing of the blue-and-yellow macaw (ara ararauna) with reference to the aerodynamics. *International Journal of Current Microbiology and Applied Sciences*, 6(8):2707–2710, August 2017.

[21] Hans Försching and Holger Hennings. Aeroelastic mysteries in avian flight. *CEAS Aeronautical Journal*, 3(2–4):135–143, November 2012.